Formation of nanogratings driven by ultrafast laser irradiation in mid-IR heavy oxide glasses

Heng Yao, Rayan Zaiter, Maxime Cavillon, Pierre Delullier, Bo Lu, Thierry Cardinal, Ye Dai, Bertrand Poumellec, Matthieu Lancry

Formation of nanogratings driven by ultrafast laser irradiation in mid-IR heavy oxide glasses

Heng Yao[1,2], Rayan Zaiter[3], Maxime Cavillon[2], Pierre Delullier[2], Bo Lu[4], Thierry Cardinal[3], Ye Dai[1,†], Bertrand Poumellec[2], and Matthieu Lancry[2,*]

[1] Department of Physics, Shanghai University, Shanghai 200444, China

[2] Institut de Chimie Moléculaire et des Matériaux d'Orsay, SP2M, CNRS, Université Paris-Saclay, 91405 Orsay, France

[3] Université de Bordeaux, CNRS, ICMCB, UPR 9048, F-33608 Pessac, France

[4] Instrumental Analysis & Research Center, Shanghai University, Shanghai 200444, China

Corresponding authors: † yedai@shu.edu.cn

* matthieu.lancry@universite-paris-saclay.fr

Abstract

This work demonstrates for the first time the formation of nanogratings inside Barium Gallo-Germanate glasses using femtosecond laser direct writing. These heavy oxide glasses, with a characterized transparency window up to 6 μm, along with the polarization sensitive birefringent nanostructures induced by femtosecond laser, offer an excellent platform for the development of mid-Infrared photonic applications. The fabricated glasses, containing both rare earth (Gd, Y) and transition metals (Zn, Ta), are directly compared to amorphous GeO_2 and commercial alumino-germanate (Corning-9754) glasses commonly used in this field. The nanogratings processing window in each glass was investigated by varying laser parameters (pulse duration, energy, repetition rate), and electron microscopy imaging directly evidenced the porous nanostructures. Among the results, a strong form birefringence in 8% ZnO-BGG glass, e.g., up to -0.029±0.001 was reported. Finally, birefringent embedded Fresnel GRIN plates were directly written in a BGG glass, to demonstrate the functionalization potential of these materials.

Keywords: Femtosecond laser; Barium gallo-germanate glass; Nanogratings; Birefringence; Photonic applications

1. Introduction

Almost two decades ago, a self-assembly phenomenon, frequently referred to Type II modifications or nanogratings (NGs), and driven by femtosecond (fs) laser irradiation, was first observed in silica bulk glass [1]. Several proposed mechanisms of NG formation include plasma interference [1], material memory effects [2,3], and interference of ultrashort-living exciton-polaritons [4]. Although still under debate, a number of intriguing properties arise from these structures, such as anisotropic light scattering, highly selective chemical etching and form birefringence associated with an extraordinary thermal stability. These properties have found practical use in microfluidics [5], polarization selective holography [6], ultrastable 5D optical memory [7,8] and 3D space variant birefringent optical devices. Until recently, the NGs formed by nanoporous structures with reduced refractive index in silica glass [9], were thought to be just observed in a handful of materials mostly limited to visible and near-Infrared (IR) range. This contrasts with the general phenomenon of laser-induced periodic surface structures (LIPSS) observed virtually on any type of material ranging from amorphous and crystalline dielectrics to semiconductors and metals [10-13]. Recently, Wang et al. [14] and Sakakura et al. [15] reported a new intermediate regime called type X modification (randomly distributed anisotropic nanopores induced by ultrafast laser), which is regarded as the early structure of NGs and can be used for ultralow-loss birefringence devices. NGs induced in volume and by fs laser were observed on several glasses or crystals among which we can cite GeO_2 glass [16-18], TeO_2 single crystal [19], Sapphire [20], Al_2O_3-Dy_2O_3 binary glass [21], lithium niobium silicate glass [22] or titanium silicate glasses (ULE, Corning) [23] and even in multicomponent aluminoborosilicate glasses (Borofloat 33, Schott) [23]. The silicate ones [24], are the most ubiquitous glasses employed for femtosecond laser direct writing (FLDW), as they are readily commercially available and offer both excellent optical transparency and physico-chemical stability. However, with respect to photonic applications, these glasses are limited to the short wavelength IR range (SWIR, < 2 μm), and do not match the increasing demand for mid-IR (ideally up to 8 μm) applications requiring 3D laser manufacturing of miniaturized, low weight and cost optical systems, for civilian (domotics, smartphone, automobile) but also security and military applications (vehicles steering, survey, weapons guidance, unmasking, countermeasure identification).

Hence, to overcome this restriction imposed by silicate glasses and access the aforementioned mid-IR range, non-silicate glass matrices must be employed, such as chalcogenides [25], fluorides [26], or heavy oxides [27]. Among these potential optical materials, heavy metal oxide glasses (HMO), and more specifically barium gallo-germanate (BGG) glasses appear as promising candidates as they are chemically stable, manufacturable by conventional means (melt-quenching), mechanically resistant [28], and can exhibit an extended transmission in the IR range up to 7-8 µm [29].

In this study, four derived BGG glasses containing transition metals (Zn, Ta), rare-earth elements (Gd, Y), and an undoped BGG glass serving as a reference (labeled Ref-BGG), were synthesized and subsequently irradiated by fs laser. Furthermore, additional studies on commercial glasses, namely SiO_2, GeO_2 and Corning 9754 (a germanate glass), were provided as comparison. The transition metals or rare-earth elements were introduced to increase the glass stability by avoiding zeolite crystal formation while maintaining a wide transparency window [30]. The Y^{3+}-containing glass was employed to describe fs laser lasing modification thresholds. The Ta^{5+}-containing glass was used due to its high bulk refractive index (e.g. GeO_2-Na_2O-Ta_2O_5 glass with high refractive index of 1.89 at wavelength of 600 nm) [31], and Gd^{3+}-containing glass for its high Verdet constant to induce Faraday electromagnetic effects. Further, ZnO was added into one conventional BGG glass to increase its chemical stability and for its excellent piezoelectric properties for potential applications. In this paper we demonstrate the formation of NGs in HMO glasses. We highlight a maximum birefringence of -0.029 for 8% ZnO-BGG sample, which is higher than that of SiO_2 (typ. up to -0.011). Furthermore, the ability to control the neutral axis orientation and to enable high refractive index contrasts led to the engineering of unique integrated optical devices with 3D spatially varying birefringence or refractive index changes. Subsequently, birefringent embedded Fresnel zone plates were demonstrated and characterized in the BGG glass.

2. Experimental

2.1 Glass synthesis

BGG glass samples were prepared through conventional melt-quenching technique from high purity reagents (Ga_2O_3: 99.999%, Fox Chemicals, GeO_2: 99.999%, Fox Chemicals, $BaCO_3$: 99.99%, Fox Chemicals, Y_2O_3: 99.9%, Alfa Aesar, Gd_2O_3: 99.999%, Alfa Aesar, Ta_2O_5: 99.993%, Alfa Aesar and ZnO: 99.999%, Alfa Aesar). The reagent grade $BaCO_3$ decomposed at high temperatures to form BaO. The powder precursors were mixed in a platinum crucible and melted at a temperature of 1550 ℃ for 1 h. The liquid was then quenched onto a metal plate to room temperature. The samples made with different chemical compositions are presented in Table 1. Additionally, a set of commercial glasses was added for comparison, namely SiO_2, GeO_2 and Corning 9754 (alumino-germanate).

Table 1 Label, molar composition, and physical characteristics of the derived BGG glass samples

Sample	Composition (Mol %)	T_g(±2°C)	T_x(±2°C)	Density (±0.01 g·cm^{-3})	n_{532} (±0.005)
Ref-BGG	$20BaO – 15Ga_2O_3 – 65GeO_2$	668	776	4.568	1.715
8% Y_2O_3-BGG	$8Y_2O_3 – 18BaO – 14Ga_2O_3 – 60GeO_2$	719	860	4.803	1.769
8% Gd_2O_3-BGG	$8Gd_2O_3 – 18BaO – 14Ga_2O_3 – 60GeO_2$	719	857	5.169	1.810
8% Ta_2O_5-BGG	$8Ta_2O_5 – 18BaO – 14Ga_2O_3 – 60GeO_2$	733	911	5.162	1.818
8% ZnO-BGG	$8ZnO – 18BaO – 14Ga_2O_3 – 60GeO_2$	639	752	4.684	1.715

2.2 Pristine glass characterization

The glass transition temperatures (T_g) and onset of crystallization (T_x) were measured by differential scanning calorimetry (DSC) and differential thermal analysis (DTA) Netzsch Pegasus 404 apparatus and with glass chunks inserted in a Pt pan, at a heating rate of 10 °C/min with a precision of ±2 °C. The density was obtained from the average of five measurements per sample using Archimedes' method by immerging a glass chunk in diethyl phthalate at room temperature on a Precisa XT 220A weighing scale with an estimated error of ±0.01 g·cm^{-3}. The refractive indices (n_d) were determined by measuring the Brewster angle at 532 nm with an estimated error of ±0.005. T_g, T_x and n_d are reported in Table 1. Micro-Raman spectra were recorded in backscattering mode on a confocal micro-Raman spectrometer (Renishaw inVia Qontor) equipped with a Synapse CCD detector using 532 nm excitation wavelength. The room temperature optical transmission measurements for each glass sample, in the UV-Visible-NIR and the IR ranges, were

respectively obtained from Agilent Cary 5000 and Bruker Equinox 55 spectrophotometers. From the attenuation measurements, the absorption coefficients (α, in cm^{-1}) of the glass samples were calculated using sample thickness of 1 mm. Note that α was obtained after calculating internal transmittance $T_{int}(\lambda)$ [32] in order to remove the Fresnel losses.

2.3 Fs-laser irradiation and characterization of modified regions

The glass samples were individually double side polished to an optical grade. A commercial Yb-doped fiber amplifier fs laser (Satsuma, Amplitude Systèmes Ltd. Pessac, France.) delivered the pulses of 1030 nm at varied pulse duration (250, 500, 800 and 1000 fs) with a typical average power up to 10 W. The beam was focused to 400 μm in depth beneath the surface of each sample using 0.6 numerical aperture (NA) aspheric lens (estimated beam waist ω_0 ~1.5 μm) and pulse repetition rate 100 kHz (except for 8% Y_2O_3-BGG glass whose pulse repetition was at 10 kHz). Furthermore, a series of rectangle patterns, 10×100 μm^2, were inscribed in all samples. Each rectangle was in fact composed of 10 lines being 100 μm long with a spacing Δy of 1 μm and a laser scanning speed of 10 μm/s (it meant 10000 pulses/μm at 100 kHz) for avoiding any diffraction effect. Moreover, the pulse energy E_p was varied from 0.025 to 3 μJ and the laser polarizations were in Xx and Xy configuration (X, laser writing orientation and x, y so-called laser polarization direction 0° and 90°, respectively) [33]. After fs laser irradiation, the inscribed sample was observed using an Olympus BX51 (Olympus, Tokyo, Japan) polarizing optical microscope equipped with "De Sénarmont" compensator which possessed a high precision quarter waveplate coupled to a rotating analyzer, providing a measurement of retardance [33]. The retardance is defined by $R = B \times l$, where B is linear birefringence (i.e. $n_e - n_o$) and l the thickness of birefringent layer induced by fs laser.

Subsequently, the structural analysis of the laser traces was carried out by performing a field-emission gun scanning electron microscope (FEG-SEM, ZEISS SUPRA 55 VP) operating in secondary electron imaging mode. The FEG-SEM allowed examining uncoated insulating or dielectric specimens using a few pA current and 1 kV accelerating voltages.

3. Results and discussions

Both the transparency in the mid-IR region (3-5 μm) and the higher nonlinear index of GeO_2 based glasses, when compared to fused silica, makes it a natural candidate or host for many applications in the near-/mid-IR region [34,35]. In particular gallo-germanate glassy systems investigated here offer the advantages of high glass transition temperatures, and an extended IR transmission window. The resulting absorption coefficient $\alpha(\lambda)$ measurements for each glass sample are presented in Fig. 1 (a). Each BGG glass presents similar optical absorption characteristics with an absorption coefficient, $\alpha < 2$ cm^{-1}, revealing a prominent optical transparency from 0.5 to 5.5 μm, hence covering the mid-IR window. One asymmetric broad absorption band could be observed around 3 μm corresponding to the hydroxyl stretching vibrations, arising from glass synthesis performed under the ambient environment. For most glasses, the IR multiphonon cut-off is made up of a peak at 6.25 μm and a strong absorption edge above 6.5 μm. Furthermore, porous nanostructures, namely NGs, are formed in our glasses upon fs laser irradiation. The morphology of these structures, along with associated fast/slow axes, are presented in Fig. 1 (b). In addition, the formed O_2– containing nanopores, as it is the case of silica glass [36] and further discussed below, agree with the results of Fig. A.1 (b) (Appendices).

Insert Fig. 1 here

The presence of laser-imprinted birefringent structures with a polarization dependent slow axis in these glasses was first characterized and measured using an Olympus BX51 polarizing optical microscope equipped with "De Sénarmont" compensator. Such a polarization-dependent birefringence is characteristic to the presence of NGs, which were further confirmed under observations made by FEG-SEM. This observation contrasts with our previous research work in similar glass matrices but with different compositions and for which NGs were not detected [37]. These derived BGG glasses include rare-earth (La^{3+}, Y^{3+}) and/or alkali (Na^{+}, K^{+}) ions. Despite a wide range of laser parameters were investigated (300-800 fs, 10-100 kHz, 1-100 μm/s), no formation (and the observation) of NGs was detected. In recent work,

it was revealed that NGs are much easier to form in glasses with a high amount of strong network former and especially in so called "long glasses" from the viscosity (T) point of view [38]. In contrast, it is very difficult to imprint NGs in "short glasses" like alkali borosilicate (BK7, Schott) or previously studied alkali BGG glasses [37].

The presently investigated derived BGG glasses were irradiated by fs laser with varying pulse energy (0.01 μJ to 5 μJ) and pulse duration (250 fs to 1000 fs). The pulse energy - pulse duration (E_p - τ_p) processing window of 8% ZnO-BGG glass is shown in Fig. 2 as an example, but the presented trends are valid for all the glass samples. The different "typical" modification regimes are clearly distinguishable: Type I (permanent isotropic refractive index), Type II (form birefringence attributed to self-assembled nanogratings) and, spatial broadening regime (laser tracks becomes much larger than the beam size) as illustrated in Fig. 4. With varying pulse duration, the onset of Type II threshold (i.e., appearance of birefringence) is found to only weakly vary, which agrees with Ref [39]. Here we highlight a relatively broad energy-pulse duration window for Type II modifications making such composition an attractive host of integrated optical devices. S. Amoruso et al. [40] have proposed an empirical scaling law of the breakdown threshold fluence $F_{th} \propto \tau_p^{0.5}$, where τ_p is the laser pulse duration. Also, Du et al. reported an increase of the thresholds with the decrease of the pulse duration for τ_p < 1 ps. This is mainly explained by an impact ionization rate scaling with the square root of the laser intensity [41,42]. Here, we reveal the Type II threshold decreases (below 800 fs) and then increases (beyond 800 fs) with pulse duration, which is only partially in agreement with the results of S. Amoruso and Du. Note that for all samples, the onset of Type II threshold is a little lower for Xx writing configuration compared to Xy configuration indicating that polarization impacts NG formation primarily at high pulse duration [43].

At short pulse duration (<350 fs), the Type I window is broad, making these fabricated glasses excellent candidates for inscription of 3D waveguides, gratings or graded index mid-IR lenses. Furthermore, the spatial broadening regime (due to heat affected zone) also presents an interest to imprint low loss single

mode or multimode waveguides with a circular profile at high speeds [44], from optimization of the index changes and mode field diameter by adjustment of exposure conditions.

The inset of Fig. 2 displays a polarized optical microscope image where a first order full waveplate is inserted, enabling the identification of the slow and fast axes of the laser tracks, indicative of the existence of Type II modifications.

Insert Fig. 2 here

To further study the impact of Type II regime formation with respect to the chemical composition in our derived BGG glasses, we investigate once again the energy vs. pulse duration landscape for Xy configuration, but this time for all the glass samples. The results are displayed in Fig. 3. Actually, all BGG glasses present similar trends on the onset energy of Type II formation, i.e., the amount of energy E_p necessary for the onset of Type II formation only slightly depends on τ_p.

- Firstly, 8% ZnO-BGG owns a progressively large Type II processing window as one increases the pulse duration up to 800 fs, e.g., from 0.075 to 1.8 μJ. There is a slight decrease observed at 1000 fs. With an increase of τ_p the Type II threshold is decreased.
- 8% Y_2O_3-BGG exhibits a similar trend with respect to 8% ZnO-BGG.
- 8% Ta_2O_5-BGG presents a similar trend as above, but goes down for long τ_p and reaches the widest Type II window at 800 fs, which extends from 0.15 to 2.8 μJ.
- Finally, 8% Gd_2O_3-BGG also presents a similar trend as referred above. Specifically, here no processing windows were found below 500 fs whereas the processing window E-τ_p is quite wide at 800 fs.
- Here GeO_2 and Ref-BGG glasses are also investigated for the sake of comparison. The Type II window of GeO_2 glass remains quite limited (typ. from 0.15 to 0.7 μJ, at 1000 fs compared to most BGG glasses including Ref-BGG (i.e., from 0.075 to 3 μJ at 1000 fs). For GeO_2, Type II threshold exhibits a slight increase in accordance with previously reported work [39]. Thus our results confirm

that derived BGG glasses are good candidates for integrated photonic components compared to GeO_2 glass.

Insert Fig. 3 here

Then the retardance R (proportional to the birefringence, B) was measured using "De Sénarmont" compensator (a quarter waveplate based technique). It is well known that the deposited energy and pulse duration are key parameters that can affect the formation of form birefringence in oxide glasses [39]. Fig. 4 exemplifies the amplitude of the retardance as a function of energy for 8% ZnO-BGG and Ref-BGG glasses in both writing configurations at 250, 500, 800 and 1000 fs. Note that repetition rate was set to 100 kHz and the writing speed to 10 µm/s resulting in a pulse density of 10,000 pulses/µm. Overall, retardance roughly increases monotonously up to a maximum and then strongly decreases for the highest energies. This corresponds to the formation of inhomogeneous and disrupted NGs that can be assigned to a significant heat accumulation at larger pulse energies [39]. Fig. 4 also shows that the minimum pulse energy required to induce detectable retardance in these derived BGG glasses is in the range of tens of nJ. As can be seen, 8% ZnO-BGG glass shows a broad Type II window at 800 fs as it is currently observed in SiO_2 or GeO_2 [45]. Moreover, we reveal that the maximum retardance in the plateauing region is increased with longer pulse duration. It can be explained by 1) an elongated focal spot yielding to longer laser tracks and 2) a lower peak power leading to a more efficient multiphoton absorption by the free electron plasma [46].

As for the dependence on polarization, both Xx and Xy writing configurations follow quite similar trends for all investigated pulse durations. Gecevičius et al. [47] have reported that Xx writing configuration would produce stronger retardance than that of Xy configuration due to the stress in and around the nanolayers, i.e. the stress-induced birefringence for a polarization perpendicular to the writing direction is stronger than for a parallel configuration [48], which is in agreement with the results in Fig. 4 (a). Interestingly, 8% ZnO-BGG exhibits a large processing window (0.35 ~ 2 µJ) at 800-1000 fs and a high retardance (up to 120 nm). Comparatively, Ref-BGG presents an even broader processing window (0.075 ~ 3 µJ) at 500-1000 fs and retardance up to 115 nm. These BGG glasses are promising hosts for polarizing devices for mid-IR

applications (bulk or fibers) since they offer a strong and controllable birefringence compared to classical IR glasses like fluoride (e.g., ZBLAN), or chalcogenide glasses where no NGs have been reported so far.

Insert Fig. 4 here

As characteristic of NGs, self-organized, and quasi-periodic nanoplanes are formed perpendicular to the laser polarization. Under adequate laser exposure conditions yielding to NGs formation, the length of the porous nanolayers zone can be measured from SEM micrographs and the resulting birefringence calculated (see Fig. 5).

Calculated birefringence values from retardance measurements, and as a function of glass composition (i.e., Corning 9754, 8% ZnO-BGG, 8% Gd_2O_3-BGG, 8% Ta_2O_5-BGG, SiO_2, GeO_2 and Ref-BGG) are presented in Fig. 5. As an illustration of the periodic structure observed in NGs using FEG-SEM imaging, the cleaved sample cross-sections of the fs laser-modified regions are presented in insets of Fig. 5. Overall, each glass exhibits similar trends so that birefringence is decreased with the length of the nanoporous zone. Firstly, 8% ZnO-BGG presents the maximum birefringence (-0.029±0.001) at 0.9 μJ among these studied glasses, which is ~2.6 times higher than that of SiO_2 (-0.011). The span of birefringence of 8% ZnO-BGG is very large (from -0.0052 to -0.0288) making it an attractive candidate for birefringence-based devices. Ref-BGG shows a birefringence up to ~-0.0123, which is as high as SiO_2 [49]. Then, the 8% Ta_2O_5-BGG irradiated sampled was found with a birefringence range between -0.004 and -0.007. These values are comparable to that of GeO_2, which is the "model glass" in the field. On the other hand, average NGs period is found to be around 240-300 nm, as shown in Fig. 5 (b)-(d), and is a function of glass composition (writing conditions: 800 fs, 1.2 μJ, Xy configuration). These results demonstrate the potential of these glasses for index-contrast devices, such as patterned waveplates, waveplates array, Fresnel zone plates and polarization gratings [50] in near-/mid-IR range.

Insert Fig. 5 here

The maximum birefringence in these derived BGG glasses along with commercial glasses (SiO_2, GeO_2 or Corning-9754 glasses) are displayed in Fig. 6 for comparison. Interestingly, the nanopores contained within

the porous nanoplanes (e.g., Xx/Xy configuration of 8% ZnO-BGG), as shown in insets of Fig. 6, and accompanied with the formation of dissolved O_2 inside these nanopores as shown by Raman spectra in supplementary information [36]. Moreover, from the down inset of Fig. 6, the mean period Λ of NGs is 201 nm. It is around or smaller than the λ/2n value and depends slightly on the pulse energy and the number of laser pulses [1]. Here n was the refractive index of these glasses measured at 550nm. Indeed, according to this expression with experimental parameters (λ = 1030 nm, n = 1.715 for Ref-BGG glass), we can obtain the average spacing equaled to 300 nm, which approached the value in our experiment.

Insert Fig. 6 here

According to the interesting characteristics of FLDW method (high flexibility, single-step, 3D), practical optical applications could be tentatively developed such as polarization-sensitive, integrated optical components and on-demand 3D micro-optics. Here, a demonstrator is fabricated in the 8% Ta_2O_5-BGG glass composition, taking the form of a single-step birefringent Fresnel zone plate with a 2 mm outer diameter and written. The design of the Fresnel GRIN plate was chosen to be a gradient thickness lens. It consists of creating a single value of refractive index variation Δn and superimposing layers of uniform index changes to create a lens in the bulk of the glass material. Here a 4 layers approach was used with 50 μm spacing between each written layer [51]. The Fresnel zones plates were optimized for a working wavelength of 632 nm. The pulse energy, pulse duration and writing speed were respectively set at 1.6 μJ, 800 fs and 0.1 mm/s, such that a π/2 phase retardation is reached at the designed wavelength for each layer and thus a maximum of 2π. In our writing conditions it takes around 5 hours for inscribing this Fresnel GRIN plate. The odd zones of embedded Fresnel zone plates exhibited in Fig. 9 (b) show strong birefringence. Finally, the written lens is characterized by measuring the primary focus at 632 nm and its waist along the defocus distance as exhibited in Fig. 9 (a). We demonstrate that the theoretical and experimental results of beam size measured at a cutoff intensity value of $1/e^2$ are in good agreement, with only 6% deviation. The typical primary focal spot is also shown in Fig. 9 (c). Overall, our investigation

proves that derived BGG glasses possess promising mid-IR optical properties and prime potential for practical applications.

Insert Fig. 7 here

4. Conclusions

Polarization dependent and birefringent nanostructures, so-called Type II modifications, were successfully imprinted by fs laser in a range of dedicated heavy oxide glasses with an emphasis on Barium Gallo-Germanate (BGG) glasses. Absorption coefficients below 1.5 cm^{-1} in the 0.25 - 5.5 μm range were obtained. SEM revealed nanostructures containing self-organized porous nanolayers associated with the formation of O_2 in the fs-laser irradiated region confirmed by Raman spectroscopy. Retardance and birefringence measurements indicated that derived BGG glasses own high birefringence values (e.g. -0.029 for 8% ZnO-BGG) compared to model glasses like SiO_2 (typ. up to -0.011) and GeO_2 (typ. up to -0.008). Moreover, a birefringent embedded Fresnel GRIN plate was successfully inscribed in the derived BGG glass as a demonstrator. The micro-engineering of optical properties in derived BGG glasses by ultrafast laser direct-writing opens the door towards new applications for mid-IR photonics among which we envision polarization maintaining waveguides, bulk retarders and their array, 3D space variant waveplates or polarization converters and more generally 3D micro-optics.

Acknowledgments

This work is financially supported by Agence Nationale de la Recherche (ANR-18-CE08-0004-01); FLAG-IR Project; National Natural Science Foundation of China (11774220, 61735010); Science and Technology Innovation Plan of Shanghai Science and Technology Commission (20JC1415700).

Disclosures

The authors declare no conflicts of interest.

References

[1] Y. Shimotsuma, P. G. Kazansky, J. Qiu, K. Hirao, Self-organized nanogratings in glass irradiated by ultrashort light pulses, Phys. Rev. Lett. 91 (2003) 247405.

[2] R. Taylor, C. Hnatovsky, E. Simova, Applications of femtosecond laser induced self-organized planar nanocracks inside fused silica glass, Laser Photon. Rev. 2 (2008) 26.

[3] V. R. Bhardwaj, E. Simova, P. P. Rajeev, C. Hnatovsky, R. S. Taylor, D. M. Rayner, P. B. Corkum, Optically Produced by Arrays of Planar Nanostructures inside Fused Silica, Phys. Rev. Lett. 96 (2006) 057404.

[4] M. Beresna, M. Gecevičius, P. G. Kazansky, T. Taylor, A. V. Kavokin, Exciton mediated self-organization in glass driven by ultrashort light pulses, Appl. Phys. Lett. 101 (2012) 053120.

[5] Y. Bellouard, A. Said, M. Dugan, P. Bado, Fabrication of high-aspect ratio, micro-fluidic channels and tunnels using femtosecond laser pulses and chemical etching, Opt. Express 12 (2004) 2120.

[6] W. Cai, A. R. Libertun, R. Piestun, Polarization selective computer-generated holograms realized in glass by femtosecond laser induced nanogratings, Opt. Express 14 (2006) 3785.

[7] Y. Shimotsuma, M. Sakakura, P. G. Kazansky, M. Beresna, J. Qiu, K. Miura, K. Hirao, Ultrafast manipulation of self-assembled form birefringence in glass, Adv. Mater. 22 (2010) 4039.

[8] J. Zhang, M. Gecevičius, M. Beresna, P. G. Kazansky, Seemingly Unlimited Lifetime Data storage in Nanostructured Glass, Phys. Rev. Lett. 112 (2014) 033901.

[9] R. Desmarchelier, B. Poumellec, F. Brisset, S. Mazerat, M. Lancry, In the heart of femtosecond laser induced nanogratings: from porous nanoplanes to form birefringence, World J. Nano Sci. Eng. 5 (2015) 115-125.

[10] A. P. Joglekar, H. Liu, G. J. Spooner, E. Meyhöfer, G. Mourou, A. J. Hunt, A study of the deterministic character of optical damage by femtosecond laser pulses and applications to nanomachining, Appl. Phys. B 77 (2003) 25-30.

[11] A. M. Ozkan, A. P. Malshe, T. A. Railkar, W. D. Brown, M. D. Shirk, P. A. Molian, Femtosecond laser-induced periodic structure writing on diamond crystals and microclusters, Appl. Phys. Lett. 75 (1999) 3716.

[12] A. Borowiec, H. K. Haugen, Subwavelength ripple formation on the surfaces of compound semiconductors irradiated with femtosecond laser pulses, Appl. Phys. Lett. 82 (2003) 4462.

[13] J. F. Young, J. S. Preston, H. M. V. Driel, J. E. Sipe, Laser-induced periodic surface structure. II. Experiments on Ge, Si, Al and brass, Phys. Rev. B 27 (1983) 1155.

[14] H. Wang, Y. Lei, L. Wang, M. Sakakura, Y. Yu, G. Shayeganrad, P. G. Kazansky, 100‐Layer Error‐Free 5D Optical Data Storage by Ultrafast Laser Nanostructuring in Glass, Laser Photon. Rev. (2022) 2100563.

[15] M. Sakakura, Y. Lei, L. Wang, Y. Yu, P. G. Kazansky, Ultralow-loss geometric phase and polarization shaping by ultrafast laser writing in silica glass, Light-Sci. Appl. 9 (2020) 15.

[16] Y. Shimotsuma, T. Asai, M. Sakakura, K. Miura, Femtosecond-laser Nanostructuring in Glass, J. Laser Micro/Nanoeng. 9 (2014) 31.

[17] F. Zhang, H. Zhang, G. Dong, J. Qiu, Embedded nanogratings in germanium dioxide glass induced by femtosecond laser direct writing, J. Opt. Soc. Am. B 31 (2014) 860.

[18] T. Asai, Y. Shimotsuma, T. Kurita, A. Murata, S. Kubota, M. Sakakura, K. Miura, F. Brisset, B. Poumellec, M. Lancry, Systematical control of structural changes in GeO_2 glass induced by femtosecond laser direct writing, J. Am. Ceram. Soc. 98 (2015) 1471.

[19] Y. Shimotsuma, K. Hirao, J. Qiu, P. G. Kazansky, Nano-modification inside transparent materials by femtosecond laser single beam, Mod. Phys. Lett. B 19 (2005) 225-238.

[20] Q. Zhai, H. Ma, X. Lin, Y. Li, W. Yin, X. Tang, X. Zeng, Y. Dai, Evolution of self-organized nanograting from the pre-induced nanocrack-assisted plasma–laser coupling in sapphire, Appl. Phys. B 127 (2021) 74.

[21] Y. Shimotsuma, S. Mori, Y. Nakanishii, E. Kim, M. Sakakura, K. Miura, Self-assembled glass/crystal periodic nanostructure in Al_2O_3-Dy_2O_3 binary glass, Appl. Phys. A 124 (2018) 82.

[22] J. Cao, L. Mazerolles, M. Lancry, F. Brisset, B. Poumellec, Modifications in lithium niobium silicate glass by femtosecond laser direct writing: morphology, crystallization, and nanostructure, J. Opt. Soc. Am. B 34 (2017) 160-168.

[23] S. Richer, C. Miese, S. Döring, F. Zimmermann, M. J. Withford, A. Trinermann, S. Notle, Laser induced nanogratings beyond fused silica-periodic nanostructures in borosilicate glasses and ULE™, Opt. Mater. Express 3 (2013) 1161.

[24] S. L. Li, P. Han, M. Shi, Y. Yao, B. Hu, M. Wang, X. Zhu, Low-loss channel optical waveguide fabrication in Nd^{3+}-doped silicate glasses by femtosecond laser direct writing, Opt. Express 19 (2011) 23958-23964.

[25] L. Liu, F. Chen, J. Cui, X. Xiao, Y. Xu, C. Hou, X. Cui, H. Guo, The mutual influence between rare earth element doping and femtosecond laser-induced effects in Ga-As-Sb-S chalcogenide glass, Ceram. Int. 47 (2021) 6388-6396.

[26] S. Gross, N. Jovanovic, A. Sharp, M. Ireland, J. Lawrence, M. Withford, Low loss mid-infrared ZBLAN waveguides for future astronomical applications, Opt. Express 23 (2015) 7946-7956.

[27] J. Bai, X. Long, X. Liu, G. Huo, W. Zhao, R. Stoian, R. Hui, G. Cheng, Embedded optical waveguides fabricated in SF10 glass by low-repetition-rate ultrafast laser, Appl. Opt. 52 (2013) 7288-7294.

[28] J. Bérubé, A. Camus, S. Messaddeq, Y. Petit, Y. Messaddeq, L. Canioni, R. Vallée, Femtosecond laser direct inscription of mid-IR transmitting waveguides in BGG glasses, Opt. Mater. Express 7 (2017) 3124-3135.

[29] W. H. Dumbaugh, J. C. Lapp, Heavy-Metal Oxide Glasses, J. Am. Ceram. Soc. 75 (1992) 2315-2326.

[30] V. M. Glazov, G. G. Timoshina, M. S. Mikhailova, A. Ta. Potemkin, Possibility of increasing the thermal stability of Si by doping with transition or rare-earth metals, Semiconductors 31 (1997) 875-878.

[31] G. Poirier, M. Dussauze, V. Rodriguez, F. Adamietz, L. Karam, T. Cardinal, E. Fargin, Second Harmonic Generation in Sodium Tantalum Germanate Glasses by Thermal Poling, J. Phys. Chem. C 123 (2019) 26528-26535.

[32] H. Hoffmann, Encyclopedia of Materials: Science and Technology, pp. 6426-6441.

[33] J. Tian, H. Yao, M. Cavillon, E. G. Caurel, R. Ossikovski, M. Stchakovsky, C. Eypert, B. Poumellec, M. Lancry, A comparison between nanogratings-based and stress-engineered waveplates written by femtosecond laser in silica, Micromachines 11 (2020) 131.

[34] S. Sakaguchi, S. Todoroki, Optical properties of GeO_2 glass and optical fibers, Appl. Opt. 36 (1997) 6809-6814.

[35] F. L. Galeener, J. C. Mikkelsen, Jr., R. H. Geils, W. J. Mosby, The relative Raman cross sections of vitreous SiO_2, GeO_2, B_2O_3, and P_2O_5, Appl. Phys. Lett. 32 (1978) 34-36.

[36] M. Lancry, B. Poumellec, J. Canning, K. Cook, J. C. Poulin, F. Brisset, Ultrafast nanoporous silica formation driven by femtosecond laser irradiation, Laser Photon. Rev. 7(6) (2013).

[37] H. Yao, R. Zaiter, M. Cavillon, B. Sapaly, F. Calzavara, P. Delullier, T. Cardinal, Y. Dai, B. Poumellec, M. Lancry, Photosensitivity of barium germano-gallate glasses under femtosecond laser direct writing for Mid-IR applications, Ceram. Int. 47 (2021) 34235-34241.

[38] Q. Xie, M. Cavillon, B. Poumellec, D. Pugliese, D. Janner, M. Lancry, A viscosity approach to the existence of nanogratings in oxide glasses, submitted to Optical Materials, Invited article.

[39] F. Zhang, A. Cerkauskaite, R. Drevinskas, P. G. Kazansky, J. Qiu, Microengineering of Optical Properties of GeO_2 Glass by Ultrafast Laser Nanostructuring, Adv. Opt. Mater. 5 (2017) 1700342.

[40] S. Amoruso, R. Bruzzese, N. Spinelli, R. Velotta, Characterization of laser-ablation plasmas, J. Phys. B: At. Mol. Opt. Phys. 32 (1999) R131-R172.

[41] D. Du, X. Liu, G. Korn, J. Squier, G. Mourou, Laser-induced breakdown by impact ionization in SiO_2 with pulse widths from 7 ns to 150 fs, Appl. Phys. Lett. 64 (1994) 3071-3073.

[42] D. Du, X. Liu, G. Mourou, Reduction of multi-photon ionization in dielectrics due to collisions, Appl. Phys. B 63 (1996) 617-621.

[43] Mindaugas Gecevičius, Doctoral Thesis, University of Southampton (Optoelectronics Research Centre) (2015).

[44] T. Gretzinger, S. Gross, M. Ams, A. Arriola, M. J. Withford, Ultrafast laser inscription in chalcogenide glass: thermal versus athermal fabrication, Opt. Mater. Express 5 (2015) 2862-2877.

[45] S. V. Lotarev, S. S. Fedotov, A. I. Kurina, A. S. Lipatiev, V. N. Sigaev, Ultrafast laser-induced nanogratings in sodium germanate glasses, Opt. Lett. 44 (2019) 1564-1567.

[46] A. Das, A. Wang, O. Uteza, D. Grojo, Pulse-duration dependence of laser-induced modifications inside silicon, Opt. Express 28 (2020) 26623-26635.

[47] M. Gecevičius, M. Beresna, J. Zhang, W. Yang, H. Takebe, P. G. Kazansky, Extraordinary anisotropy of ultrafast laser writing in glass, Opt. Express 21 (2013) 3959-3968.

[48] A. Champion, M. Beresna, P. Kazansky, Y. Bellouard, Stress distribution around femtosecond laser affected zones: effect of nanogratings orientation, Opt. Express 21 (2013) 24942-24951.

[49] M. Beresna, M. Gecevičius, M. Lancry, B. Poumellec, P. G. Kazansky, Broadband anisotropy of femtosecond laser induced nanogratings in fused silica, Appl. Phys. Lett. 103 (2013) 131903.

[50] T. Todorov, L. Nikolova, N. Tomova, Polarization holography. 2: Polarization holographic gratings in photoanisotropic materials with and without intrinsic birefringence, Appl. Opt. 23 (1984) 4588-4591.

[51] K. Yamada, W. Watanabe, Y. Li, K. Itoh, J. Nishii, Multilevel phase-type diffractive lenses in silica glass induced by filamentation of femtosecond laser pulses, Opt. Lett. 29 (2004) 1846-1848.

Figure captions:

Figure 1 (a) Absorption coefficient of Ref-BGG, 8% Gd_2O_3-BGG, 8% Ta_2O_5-BGG, 8% Y_2O_3-BGG, 8% ZnO-BGG and Corning-9754 glasses as a function of wavelength. (b) Sketch of femtosecond laser induced nanogratings in bulk glass. The optical axis of the self-organized nanostructures is perpendicular to the self-organized nanoplanes with t_1 the nanoplane thickness and t_2 the period. n_1 and n_2 are the corresponding refractive index indices.

Figure 2 Energy vs. pulse duration landscape showing the various fs laser transformation regimes encountered in the experimental conditions: no modification, Type I, Type II and spatial broadening regime. The selected sample is 8% ZnO-BGG with Xx (a) and Xy (b) configurations, respectively. Inset shows the polarized optical microscope image (bottom light illumination) with crossed polarizers and a full waveplate inserted at 45°.

Figure 3 Energy vs. pulse duration showing the Type II processing window of glass groups in Xy configuration: (a) GeO_2, 8% Y_2O_3-BGG and 8% ZnO-BGG glasses; (b) 8% Gd_2O_3-BGG, 8% Ta_2O_5-BGG and Ref BGG glasses. Numbers on the graphs correspond to pulse energy values.

Figure 4 Mean retardance of laser-written structures as a function of pulse energy and pulse duration (250, 500, 800 and 1000 fs) for (a) 8% ZnO-BGG glass and (b) Ref-BGG glass. The insets indicate typical modification regimes: Type I, Type II, and spatial broadening regimes. The laser parameters were 1060 nm, 0.6 NA, 100 kHz for 8% ZnO-BGG.

Figure 5 Birefringence as a function of porous nanolayers length for Corning 9754, 8% ZnO-BGG, 8% Gd_2O_3-BGG, 8% Ta_2O_5-BGG, SiO_2, GeO_2 and Ref-BGG glasses. 3 insets of FEG-SEM secondary electron micrographs of the cleaved surfaces of laser traces cross sections for (b) 8% ZnO-BGG; (c) 8% Ta_2O_5-BGG; (d) 8% Gd_2O_3-BGG. The red and green arrows indicate the laser polarization and laser scanning directions, respectively. For simply presenting birefringence evolution, we use the positive birefringence values (Note all the birefringence values are negative due to the characteristics of uniaxial negative birefringence of NGs).

Figure 6 Birefringence range as a function of refractive index (measured at 550nm) for various glass samples at 800 fs in Xx configuration (left bar) and Xy configuration (right bar). Additional insets show FEG-SEM secondary electron images

of 8% ZnO-BGG in Xx and Xy configurations, respectively. For simply presenting birefringence evolution, we use the positive birefringence values (Note all the birefringence values are negative due to the characteristics of uniaxial negative birefringence of NGs).

Figure 7 (a) Beam size at $1/e^2$ (μm) vs. defocus (mm) with experimental and theorical radius values. (b) Microscope image of fs inscribed Fresnel zone plate. (c) Image of the primary focus at 632 nm in the 8% Ta_2O_5-BGG glass sample.

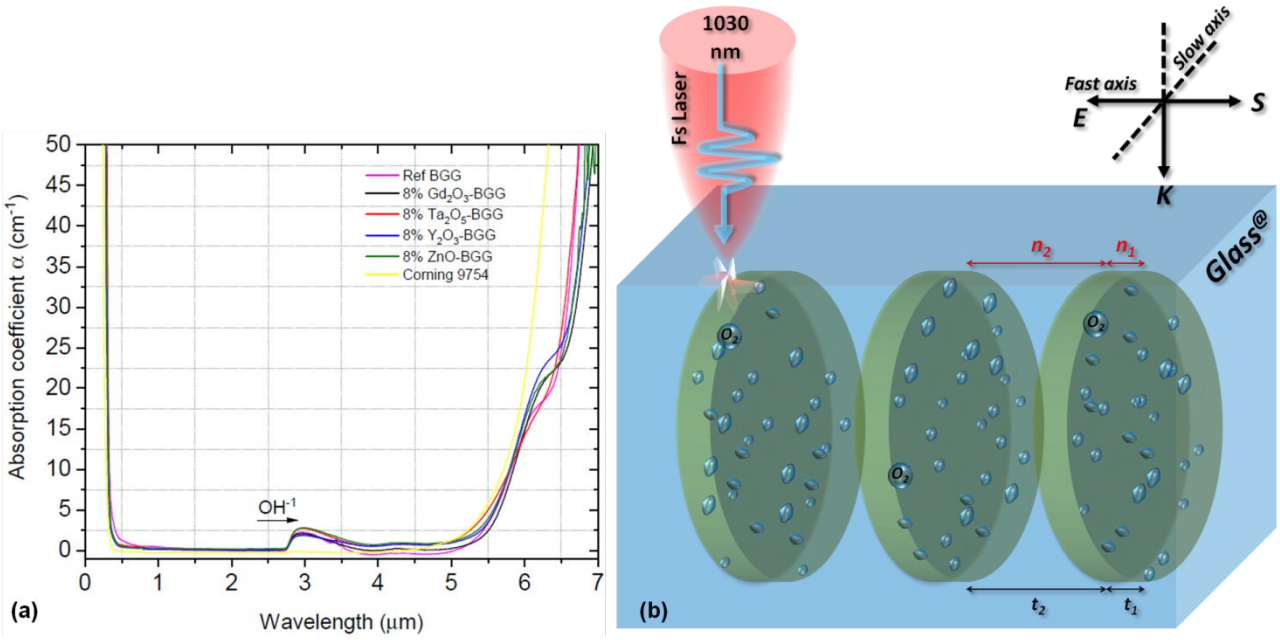
Absorption coefficient α (cm⁻¹)
Wavelength (μm)
Ref BGG
8% Gd2O3-BGG
8% Ta2O5-BGG
8% Y2O3-BGG
8% ZnO-BGG
Corning 9754
OH-1
(a)
1030 nm
Fs Laser
Fast axis
Slow axis
E
S
K
n2
n1
Glass@
O2
t2
t1
(b)

Figure 1

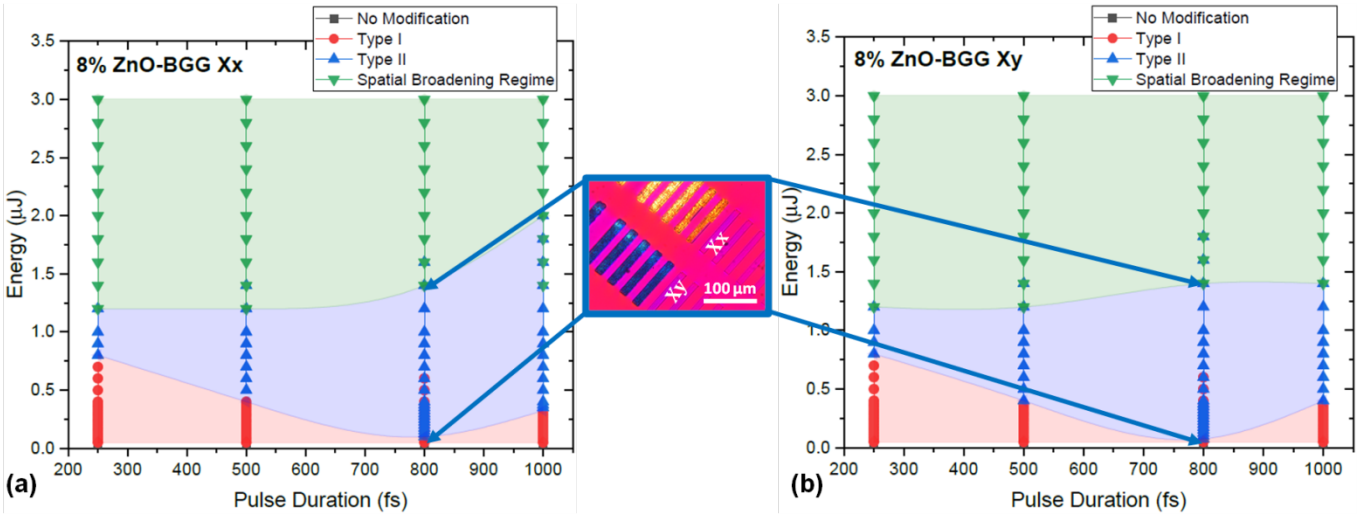
8% ZnO-BGG Xx
No Modification
Type I
Type II
Spatial Broadening Regime
Energy (μJ)
Pulse Duration (fs)
(a)
Xy
Xx
100 μm
8% ZnO-BGG Xy
No Modification
Type I
Type II
Spatial Broadening Regime
Energy (μJ)
Pulse Duration (fs)
(b)

Figure 2

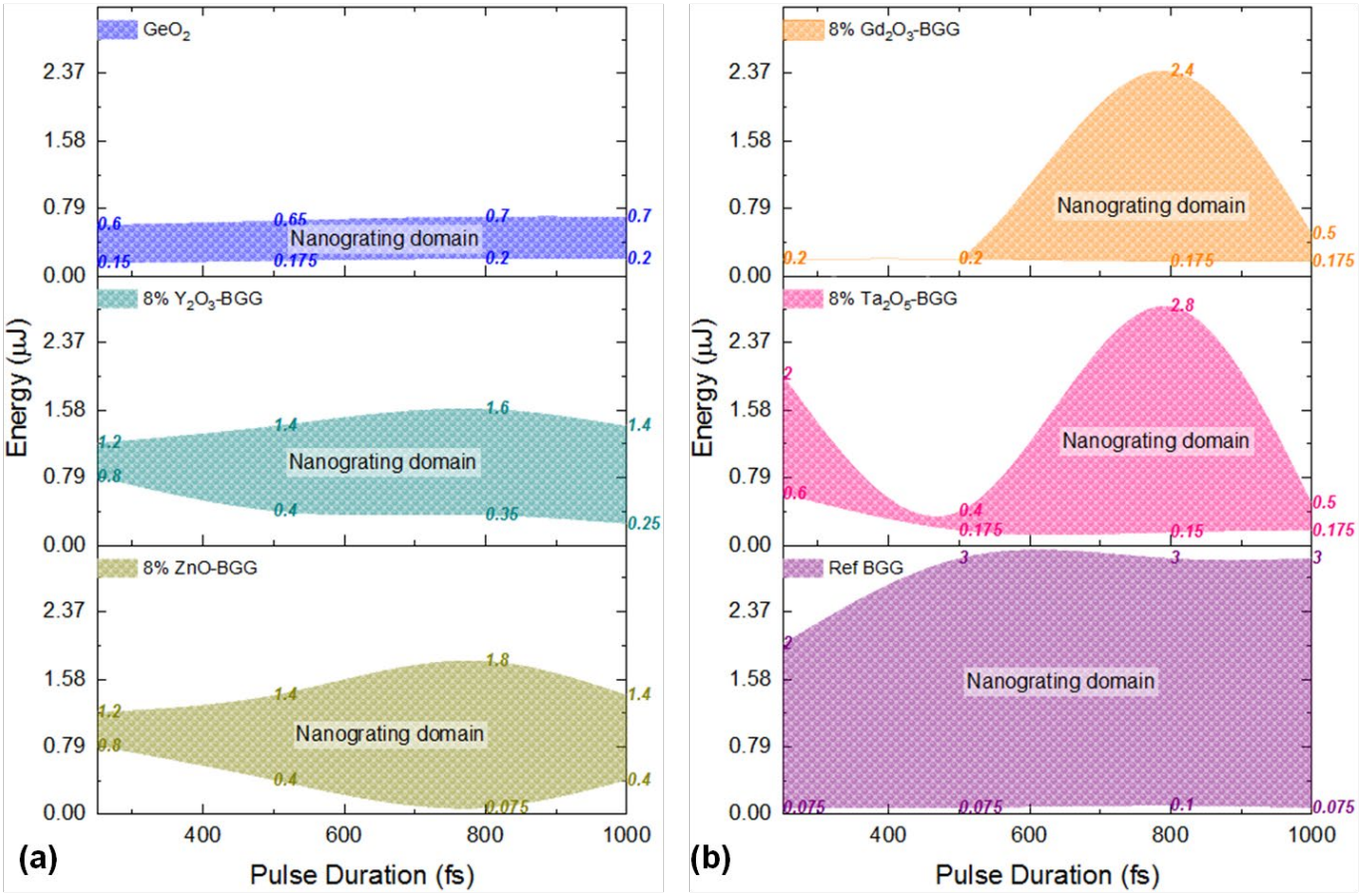
GeO2
8% Y2O3-BGG
8% ZnO-BGG
8% Gd2O3-BGG
8% Ta2O5-BGG
Ref BGG
Nanograting domain
Energy (μJ)
Pulse Duration (fs)
(a)
(b)

Figure 3

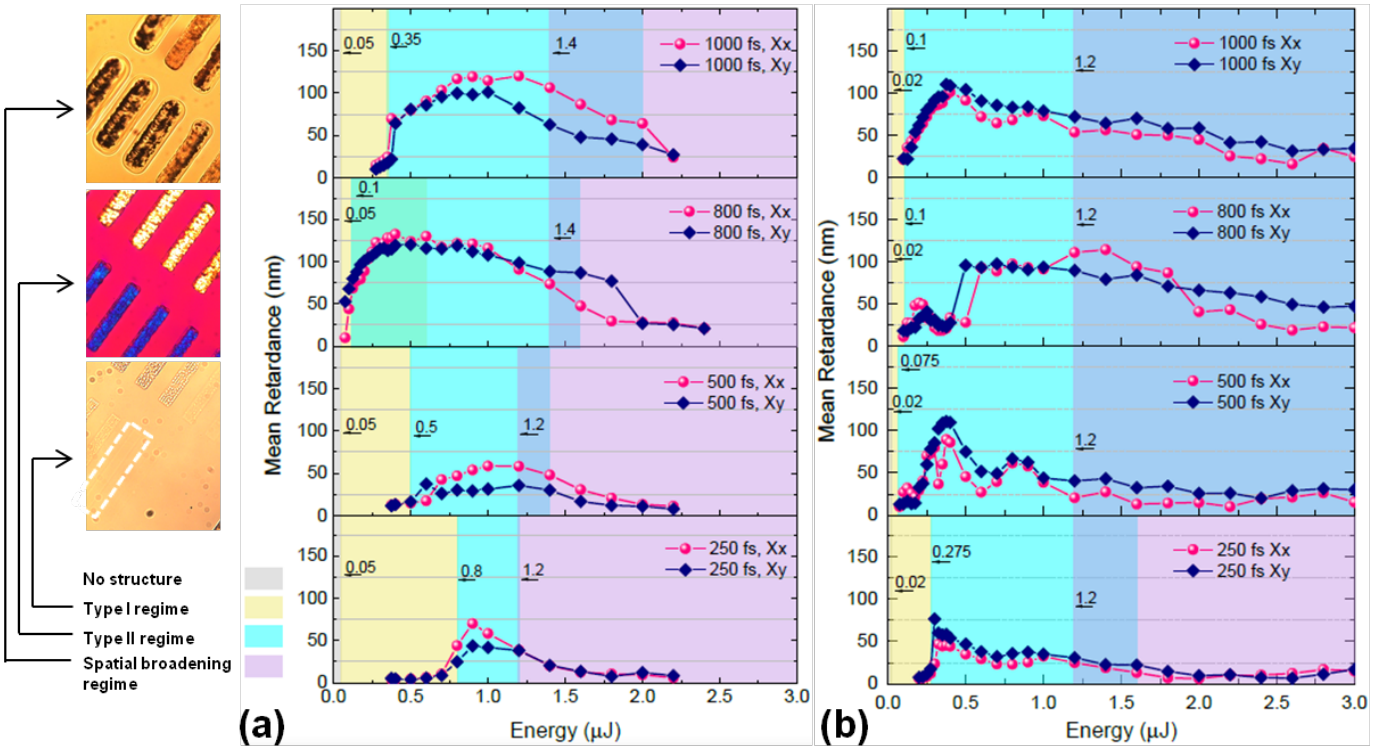
No structure
Type I regime
Type II regime
Spatial broadening regime
Mean Retardance (nm)
Energy (μJ)
(a)
(b)
1000 fs, Xx
1000 fs, Xy
800 fs, Xx
800 fs, Xy
500 fs, Xx
500 fs, Xy
250 fs, Xx
250 fs, Xy
1000 fs Xx
1000 fs Xy
800 fs Xx
800 fs Xy
500 fs Xx
500 fs Xy
250 fs Xx
250 fs Xy

Figure 4

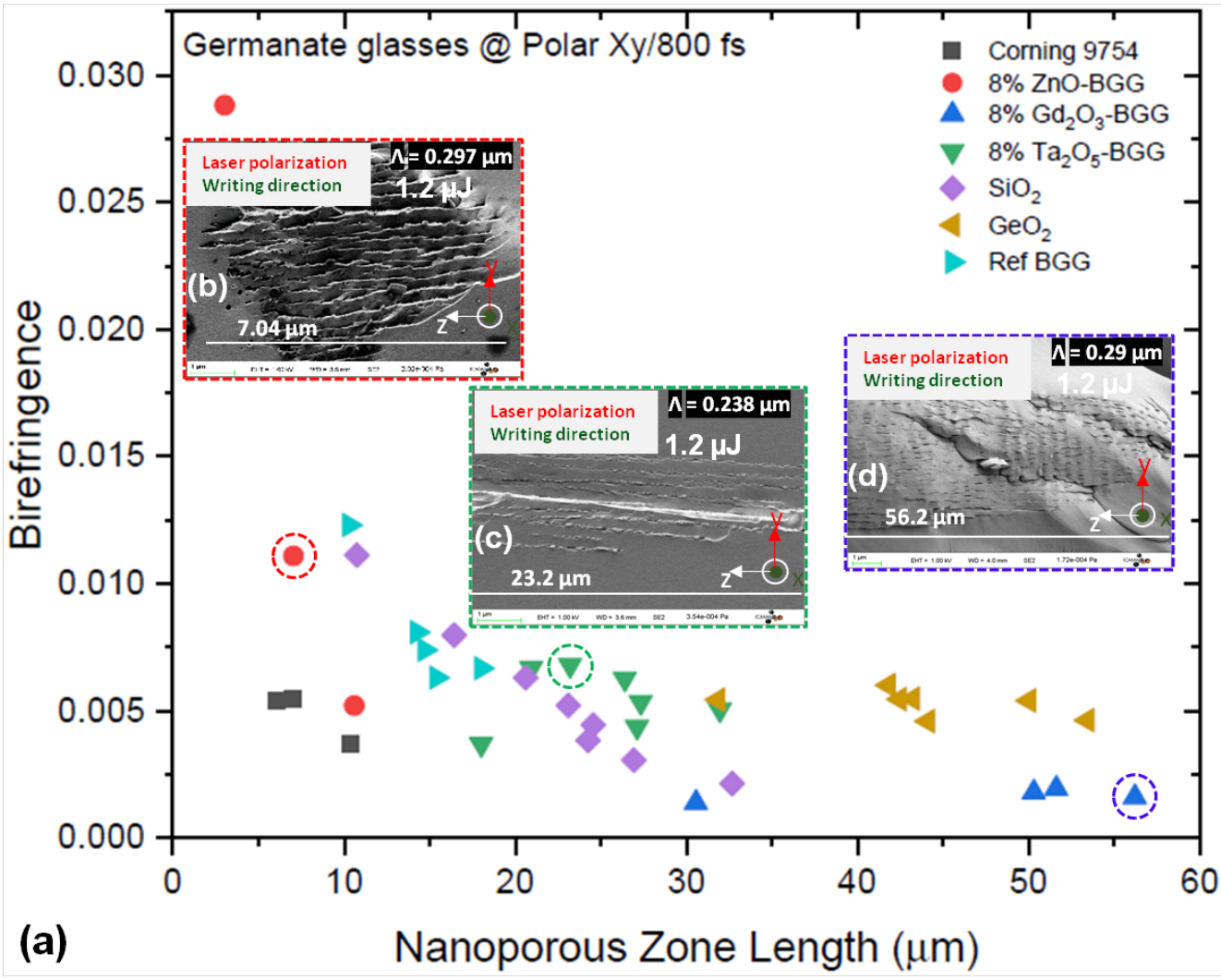
Germanate glasses @ Polar Xy/800 fs
Corning 9754
8% ZnO-BGG
8% Gd_2O_3-BGG
8% Ta_2O_5-BGG
SiO_2
GeO_2
Ref BGG
Laser polarization
Writing direction
Λ= 0.297 µm
1.2 µJ
(b)
7.04 µm
Laser polarization
Writing direction
Λ = 0.238 µm
1.2 µJ
(c)
23.2 µm
Laser polarization
Writing direction
Λ= 0.29 µm
1.2 µJ
(d)
56.2 µm
Birefringence
0.000
0.005
0.010
0.015
0.020
0.025
0.030
0
10
20
30
40
50
60
(a)
Nanoporous Zone Length (µm)

Figure 5

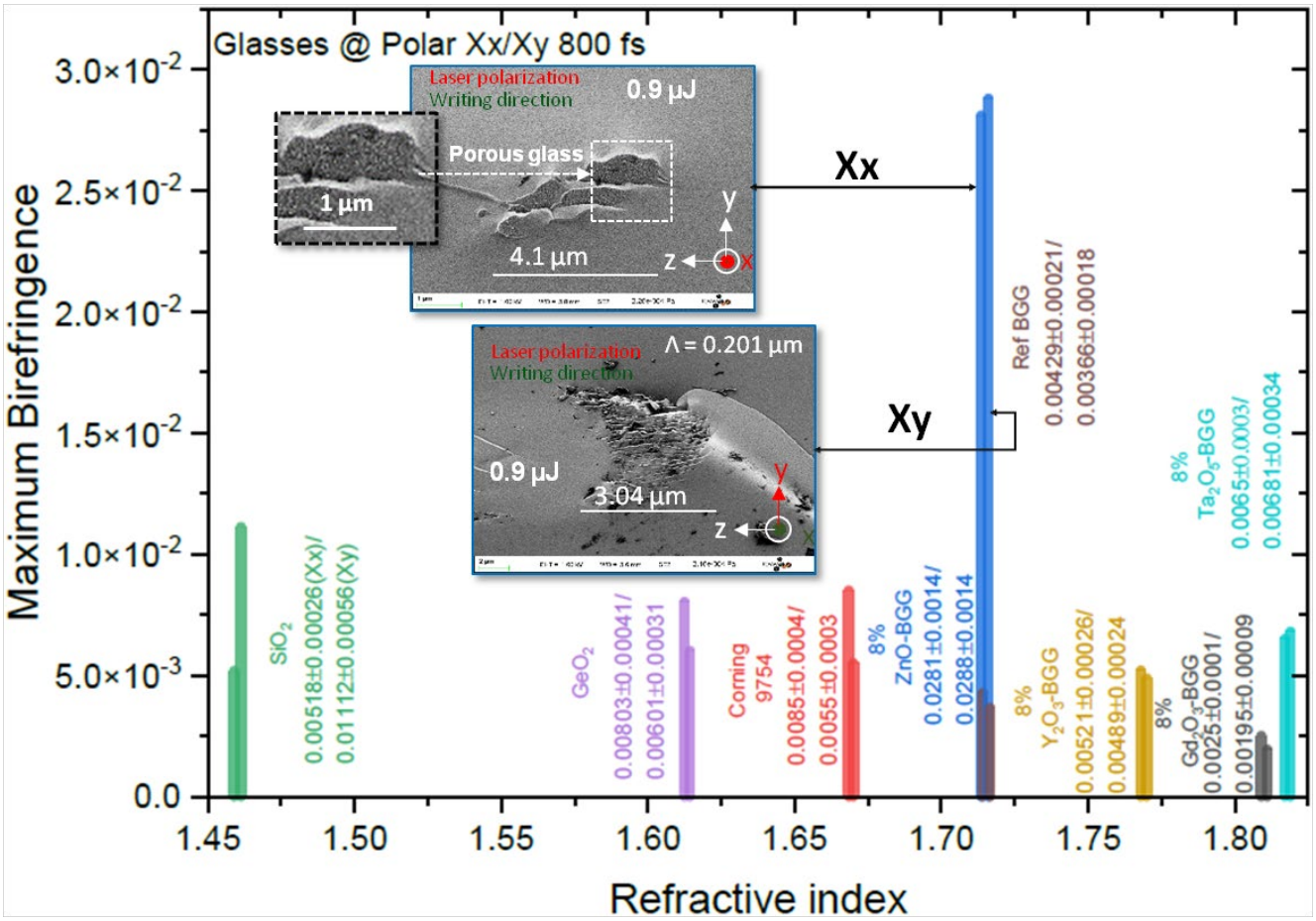
Glasses @ Polar Xx/Xy 800 fs
Maximum Birefringence
Refractive index
Laser polarization
Writing direction
0.9 µJ
Porous glass
1 µm
4.1 µm
Xx
Xy
Λ = 0.201 µm
3.04 µm
SiO2
0.00518±0.00026(Xx)/
0.01112±0.00056(Xy)
GeO2
0.00803±0.00041/
0.00601±0.00031
Corning
9754
0.0085±0.0004/
0.0055±0.0003
8%
ZnO-BGG
0.0281±0.0014/
0.0288±0.0014
Ref BGG
0.00429±0.00021/
0.00366±0.00018
8%
Y2O3-BGG
0.00521±0.00026/
0.00489±0.00024
8%
Gd2O3-BGG
0.0025±0.0001/
0.00195±0.00009
8%
Ta2O5-BGG
0.0065±0.0003/
0.00681±0.00034

Figure 6

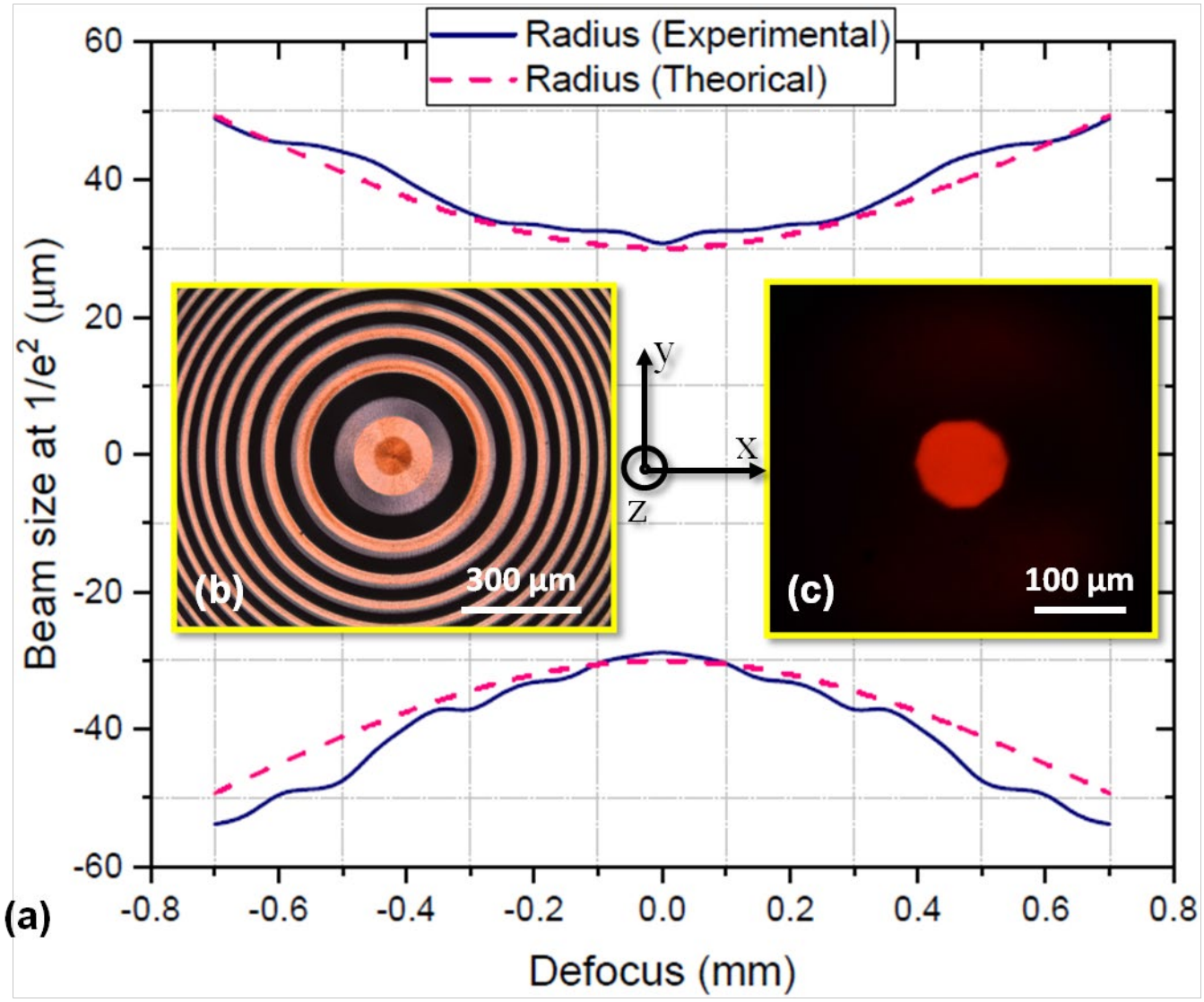
Radius (Experimental)
Radius (Theorical)
Beam size at 1/e² (μm)
Defocus (mm)
(a)
(b)
300 μm
(c)
100 μm
y
x
z
60
40
20
0
-20
-40
-60
-0.8
-0.6
-0.4
-0.2
0.0
0.2
0.4
0.6
0.8

Figure 7

Supplementary material:

Formation of nanogratings driven by ultrafast laser irradiation in mid-IR heavy oxide glasses

Heng Yao[1,2], Rayan Zaiter[3], Maxime Cavillon[2], Pierre Delullier[2], Bo Lu[4], Thierry Cardinal[3], Ye Dai[1,†], Bertrand Poumellec[2], and Matthieu Lancry[2,*]

[1] Department of Physics, Shanghai University, Shanghai 200444, China

[2] Institut de Chimie Moléculaire et des Matériaux d'Orsay, SP2M, CNRS, Université Paris-Saclay, 91405 Orsay, France

[3] Université de Bordeaux, CNRS, ICMCB, UPR 9048, F-33608 Pessac, France

[4] Instrumental Analysis & Research Center, Shanghai University, Shanghai 200444, China

Corresponding authors: † yedai@shu.edu.cn

* matthieu.lancry@universite-paris-saclay.fr

Appendices

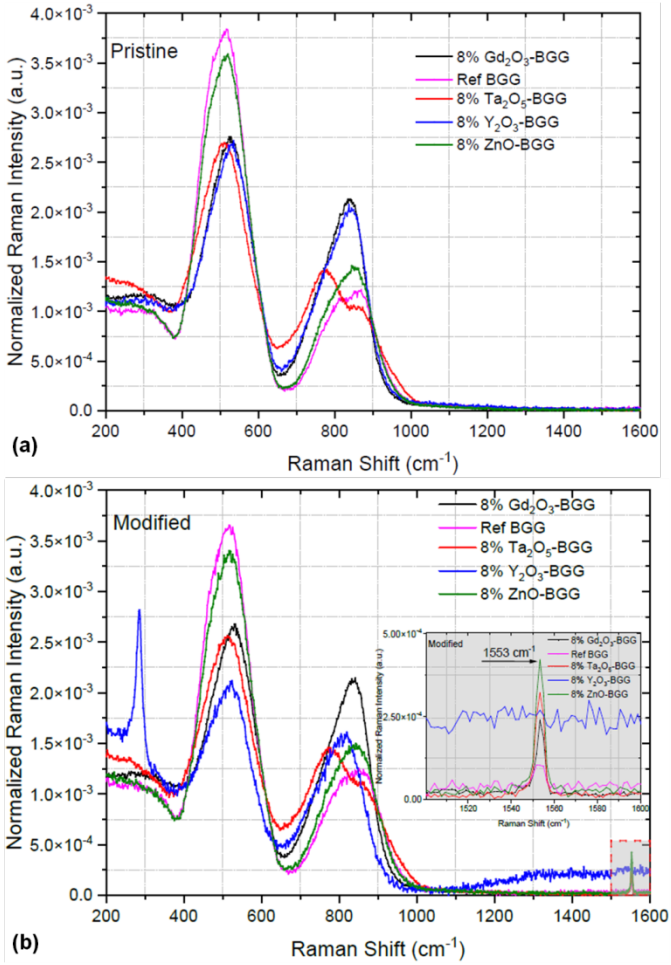

Fig. A1. (a) Normalized Raman intensity of 8% Gd_2O_3-BGG, Ref-BGG, 8% Ta_2O_5-BGG, 8% Y_2O_3-BGG and 8% ZnO-BGG pristine glasses as a function of Raman shift. (b) Normalized Raman intensity of 8% Gd_2O_3-BGG, Ref-BGG, 8% Ta_2O_5-BGG, 8% Y_2O_3-BGG and 8% ZnO-BGG fs-laser modified glasses as a function of Raman shift, writing conditions: 800 fs, 1 µJ, Xx configuration.

The Raman spectra normalized to the total scattered intensity cross-section from 200 to 1600 cm^{-1} are displayed in Fig. A1(a) for each pristine glass sample. The Raman spectra confirm the glass nature of all samples. As shown in Fig. A1(b), each fs-laser modified derived BGG glass exhibits similar Raman spectrum features with respect to the pristine Ref-BGG glass excepted for 8% Y_2O_3-BGG which presents probably a partial crystallization indicated by

the peak at 280 cm^{-1}. Generally, features at low frequencies, namely below 300 cm^{-1}, are attributed to network-modifying cation vibrations in large interstitial sites or to acoustic modes involving motions of the tetrahedral cations in large atom clusters [1]. Furthermore, it is well known that the Raman shift at 1553 cm^{-1} is related to formation of molecular oxygen, O_2 [2] indicating the breakdown of T-O-T (T= Ge or Ga). Here it can be explained that thanks to the strong intensity of ultrafast laser, Ge-O bonds are decomposed i.e., oxygen is displaced from Ge-O-Ge bond and leave an ODC together with an interstitial oxygen. This is initiated in a fraction of ps and a few separated pulses, electrons excited by MPI are trapped in glasses and then form self-trapped exciton (STE), and after STE relaxation, the interstitial oxygen atoms combine and are neutralized to form dissolved O_2 mostly inside the nanopores [2], as exemplified in the inset of Fig. 6. For more details on the characteristic features of the absorption and Raman spectra in these similar family glasses, the Reader is directed to the Refs [3,4].

References

[1] D. A. Mckeown, C. I. Merzbacher, Raman spectroscopic studies of $BaOGa_2O_3GeO_2$ glasses, J. Non-Cryst. Solids 183 (1995) 61-72.

[2] M. Lancry, B. Poumellec, J. Canning, K. Cook, J. C. Poulin, F. Brisset, Ultrafast nanoporous silica formation driven by femtosecond laser irradiation, Laser & Photon. Rev. 7(6) (2013).

[3] H. Yao, R. Zaiter, M. Cavillon, B. Sapaly, F. Calzavara, P. Delullier, T. Cardinal, Y. Dai, B. Poumellec, M. Lancry, Photosensitivity of barium germano-gallate glasses under femtosecond laser direct writing for Mid-IR applications, Ceram. Int. 47 (2021) 34235-34241.

[4] T. Guérineau, C. Strutynski, T. Skopak, S. Morency, A. Hanafi, F. Calzavara, Y. Ledemi, S. Danto, T. Cardinal, Y. Messaddeq, Extended germano-gallate fiber drawing domain: from germanates to gallates optical fibers, Opt. Mater. Express 9 (2019) 2437-2445.